Two-Photon Imaging of the Immune System: A Custom Technology Platform for High-Speed, Multicolor Tissue Imaging of Immune Responses

Andrew Bullen, Rachel S. Friedman, and Matthew F. Krummel

Contents

Abstract Modern imaging approaches are proving important for addressing contemporary issues in the immune system. These approaches are particularly useful for characterizing the complex orchestration of immune responses *in vivo*. Multicolor, two-photon imaging has been proven to be especially enabling for such studies because of its superior tissue penetration, reduced image degradation by light scattering leading to better resolution and its high image quality deep inside tissues. Here, we examine the functional requirements of two-photon imaging instruments necessary for such immune studies. These requirements include frame rate, spatial resolution and the number of emission channels. We use this discussion as a starting point to compare commercial systems and to introduce a custom technology platform that meets these requirements. This platform is noteworthy because it is very cost-effective, flexible and experimentally useful. Representative data collected

A. Bullen (✉), R.S. Friedman, and M.F. Krummel
Department of Pathology and Biological Imaging Development Center, University of California San Francisco, 513 Parnassus Ave, San Francisco, CA 94143-0511, USA
e-mail: Andrew.Bullen@ucsf.edu or Matthew.Krummel@ucsf.edu

D. McGavern and M. Dustin (eds.), *Visualizing Immunity,* Current Topics in Microbiology and Immunology 334,
DOI: 10.1007/978-3-540-93864-4_1, © Springer-Verlag Berlin Heidelberg 2009

with this instrument is used to demonstrate the utility of this platform. Finally, as the field is rapidly evolving, consideration is given to some of the cutting-edge developments in multiphoton microscopy that will likely improve signal strength, depth penetration and/or the experimental usefulness of this approach.

1 Introduction

Direct imaging of the individual cell types of the immune system in their native context undeniably provides the most accurate spatiotemporal assessment of the system-wide properties of the immune response. Over the past 6 years, this technique has increasingly been facilitated by imaging methods utilizing two-photon laser-scanning microscopy (TPLSM) (Cahalan and Parker 2008). Unlike other methods, the behavior of individual cells are observed via this technology in an largely intact microenvironment containing, by definition, physiological concentrations of soluble mediators, growth factors, as well as cell–cell contacts with other components of the system.

Central to this is the ability of multiphoton excitation to provide improved depth penetration and reduced phototoxicity over longer observation periods (Cahalan et al. 2002; Williams et al. 2001), which is a key aspect to observing biology over time within healthy tissues. To achieve such observational accuracy, however, is not without challenges. These include proper experimental design to highlight specific cells without perturbing the overall biology, optimal sample preparation to minimize artifacts due to whole animal surgery and, of course, the best possible instrumentation for detecting optical signals from the deepest possible location within complex organs. This latter component is an area of intense development and an area whose improvement simplifies experimental and sample-preparation considerations. In this review, we will highlight the optical and instrumentation approaches that are improving this technology, and compare a variety of TPLSM implementations used in immune-imaging. As an example of a custom system that has been highly successful in imaging immune responses, we will elaborate the details of a custom-instrument that we have implemented, and which is increasingly being adopted for its relative ease of implementation, flexibility, cost, and importantly, imaging quality. Finally, we will describe emerging technologies and how they are likely to improve spatial and temporal aspects of this approach.

1.1 The Power of Imaging for Addressing Issues/Answering Questions in the Immune System

What are the benefits of live-cell imaging in the immune response, generally? Studies undertaken by Wülfing and Davis (Wülfing et al. 1997), Delon and Trautmann (Delon et al. 1998), Negulescu and Cahalan (Negulescu et al. 1996)

and Dustin and Unanue (Dustin et al. 1997) in the mid-1990s highlighted the distinct power of observing single cell dynamics with reference to the calcium response. Notably, all these groups were able to take advantage of the fact that imaging single-cell dynamics permits the direct observation of an activation 'timeline'. In particular, they were to observe each cell from the start of its interaction with an antigen-presenting cell, followed by the full course of activation and calcium influx dynamics as it related to cell shape change and motility arrest (Negulescu et al. 1996; Dustin et al. 1997; Delon et al. 1998), and subsequently how it was influenced by the nature of antigen-presenting cells (APC) (Delon et al. 1998) and peptide–MHC complexes (pMHC) (Wülfing et al. 1997).

The imaging of single events in their entirety provides clear benefits over other 'bulk' methods such as flow cytometry for observing kinetic relationships since it avoids the 'temporal smear' generated by variations in the population behavior. Take, for example, the onset, magnitude, and duration of calcium signaling in a population of cells. A variation within the population in any of these parameters can be both observed and normalized when all cells are measured in their entirety during the period of interest. In contrast, a bulk measurement of the population over time simply measures the average behavior. If there is great variation in any of the kinetic parameters, the maximum magnitude of the others can be misrepresented due to contributions from cells that are at different stages of the response. Analysis of single cells allows all parameters to be viewed in their direct relationship to each other (i.e., in the recording of each single cell). These can later be pooled by common feature for statistical analysis (e.g., always starting at the time of onset of the responses), thus providing dramatically improved details of downstream kinetic relationships within the population.

The direct observation of cells undergoing biological activity using real-time microscopy also provides important spatial information. This information can help describe subcellular events and/or characterize the local microenvironment. In the first case, direct imaging of immune cells *in vitro* permits subcellular analysis of responses, such as the very early imaging of antibody-driven calcium influx within cytotoxic T lymphocytes (CTLs). Such observations have provided evidence that much of the influx was polarized, emanating from a single side of the cell (Poenie et al. 1987). This is now known to represent release of intracellular calcium stores, often from polarized endoplasmic reticulum (ER). Similarly, the movement of subcellular signaling molecules within cells, tagged with GFP, permits the assembly of a wide variety of signaling complexes to be analyzed with reference to calcium signaling, morphology, and/or motility (Krummel et al. 2000; Schaefer et al. 1999; Bunnell et al. 2001; Varma et al. 2006; Yokosuka et al. 2005). In the second case, cellular behavior in complex tissues is not constant but rather varies depending on local factors such as the presence of chemokines. For example, naive T cells arrest more on dendritic cells (DC) that are already involved in activation via other T cells (Hugues et al. 2007; Castellino et al. 2006). This type of problem, in particular, has benefited from multiphoton imaging of immune responses *in vivo*.

Within this area, multiphoton microscopy has, or is poised, to address the following types of questions with respect to cellular activation:

- What are the single-cell dynamics of activation? For example, Miller and Cahalan (Miller et al. 2002, 2004), and Mempel and von Andrian (Mempel et al. 2004) have shown that T cells undergo activation in multiple phases, corresponding to initial scanning of antigen-bearing surfaces and culminating in firm arrest of T cells on activated DCs.
- Where does activation occur spatially within a given tissue? For example, it was found that B cells can be activated on DCs, following entry into the lymph node, and as they traverse the T cell zone rather than solely in B cell zone (Qi et al. 2006).
- What is the effect of the spatial milieu (different microenvironments or different tissues)? For example, activating B cells near the B cell zone/T cell zone junction are sensitive to a chemokine gradient in that zone which attracts them toward the T cell zone. In contrast, more distal cells show no evidence of motion toward this potential source of T cell 'help' (Okada et al. 2005).
- Which cell types are present during an immune response *in vivo* and how do they contribute? For example, DCs have been highlighted to be the partners for T cell activation using chemical dye-labeling *in vivo* (Miller et al. 2004), dye-labeling prior to their adoption (Mempel et al. 2004; Bousso and Robey 2003), antibody-labeling *in vivo* (Hugues et al. 2004), and genetic marking (Lindquist et al. 2004; Shakhar et al. 2005).

Multiphoton microscopy has the potential to produce multiple types of readouts. Currently, a majority is limited to determinations of cell–cell interactions and positional detail although improving instrumentation is now permitting greater use of subcellular markers. Such resolution and sensitivity will begin to allow direct measurements of signaling protein aggregation, endocytosis, exocytosis, and polarity, in addition to the creation of custom biosensors to report on specific signaling cascades. Some of the most frequently applied include:

- Cell arrest. For example, the arrest of T cells following exposure to antigen (Miller et al. 2002; Bousso and Robey 2003).
- Cell morphology. For example, T cells undergoing motility tend to do so in a hand-mirror morphology, similar to amoeba (Miller et al. 2002).
- Calcium influx. For example, B cells encountering antigen-bearing DCs upon entry into the lymph node can be observed to flux calcium as measured by Fluo4 (Qi et al. 2006). This method is limited at present as the fluorescent dyes for these types of studies are rapidly vesicularized.
- Cell–cell association (or persistence). For example, T cells activating in a lymph node often do so in 'clusters' (Bousso and Robey 2003; Tang et al. 2006; Beuneu et al. 2006; Sabatos et al. 2008) and such clusters can permit long-lived cell–cell contacts between adjacent cells leading to directed cytokine secretion (Sabatos et al. 2008).
- Subcellular analysis of particle distribution. For example, antigens taken up by macrophages in the cortical sinus are distributed within subcellular compartments there (Phan et al. 2007).

1.2 Functional Requirements for Imaging Immune Function In Vivo

Leukocytes have defined characteristics that define the requirements for imaging events *in vivo*. On the one hand, the immune system is highly motile and thus requires sufficiently fast sampling to quantify this motion. In addition, this is a system containing multiple cell types and, thus, requires multiple labeling and detection strategies to differentiate cell types. It is also not limited in its activity to the surface of tissues or organs – in fact the cells of the immune system can lie deep within tissues, surveying for or defending against foreign organisms.

Functional requirements that need be considered for imaging are speed of sampling, sensitivity of detection, particularly with reference to depth penetration, multicolor acquisition, and the tradeoff between all of these and microscopic spatial resolution and macroscopic field of view (FOV).

1.2.1 Frame-Rate and Speed of Acquisition Considerations

Lymphocytes, key players in the immune responses, are intrinsically motile, with center-of-mass displacements that reach >25 μm min^{-1} (Miller et al. 2002). In addition, projections from the lymphocyte surface can appear and significantly change within seconds. As the path taken by T cells is rarely linear in tissues such as lymph nodes but more closely resembles a 'random walk' (Miller et al. 2002) (though it is not likely to be truly 'random'; Bajenoff et al. 2006), higher sampling frequencies are essential to provide an accurate readout of instantaneous velocities. Regardless of the underlying guiding force for movement, it is clear that sampling frequency plays a large part in determining the accuracy of a measurement of velocity, particularly when cells are persistent for only a finite period of time. A brief practical measure is that the sampling interval t should be considerably less than the persistence time P.

As an illustrative example, consider theoretical displacements based on motion described by a typical equation for a Persistent Random Walk (Othmer et al. 1988):

$$< d(t)^2 > = nS^2 \, [Pt - P^2 \, (1 - e^{-t/P}),$$

where $d(t)$ is the observed displacement, n is the number of dimensions, S is the speed, and P is the persistence (period of time without a turn). When the observed time period is less than the cellular directional persistence time ($t < P$), the equation reduces to:

$$d\,(t) = St$$

which is to say that the observed displacement is closely approximated by measures of speed multiplied by time. This is the ideal measurement scenario – that the measured displacement is in fact an accurate measure of the true instantaneous velocities.

For a theoretical cell with persistence of 2 min whose behavior followed this type of description (S set to 10), measurements at 30-s intervals ($P > t$) would yield displacement values of 5.8 μm/30 s and therefore velocities of 11.6 μm min^{-1}. Intervals of collection of 2 min ($P = t$) would on average obtain measurements of "instantaneous velocities" as ~21 μm 2 min^{-1} or 10.5 μm min^{-1}. Further reduced sampling rates of 4 and 10 min intervals ($P < t$) would on average obtain measurements of "instantaneous velocities" as 8.7 and 6.9 μm min^{-1}, respectively. The true magnitude of the errors obviously depends upon the underlying biology and doubtless adheres to a significantly more complex description. Indeed, there are a plethora of variations of models for modeling cell motility (Codling et al. 2008). However, this example serves to indicate the value of fast sampling in theory, but may also indicate a practical explanation for modest differences in reported motility parameters for naive T lymphocytes depending upon the frame-rate of data acquisition.

In practice, lymphocytes can cover considerable distances during a short time course of analysis. This in turn creates the important consideration of total X–Y–Z FOV since one cannot track a cell that has left the observation volume. Practically, this will create conflicts with requirements for spatial resolution, since complete sampling of a larger volume can either be done by capturing more pixels (longer collection times) or with the same number of larger pixels. Practically, this often entails variations in the number of Z-slices that are collected since varying this parameter can quickly multiply the time taken to acquire data. For example, presuming 30 z-stacks are required to capture a sufficient volume of data for analysis, 3-s acquisition times result in a full 90 s-between frames, thus potentially underrepresenting the very fastest movements as described above. Lowering spatial resolution in the *Z*-axis by taking larger Z-steps may initially appear an attractive way to minimize these bottlenecks. However, the resulting decrease in ability to accurately assess the cell center of mass in the *Z*-axis results in inaccurate high and low velocities being reported and, more generally, a broadening of the velocity distribution. A more detailed analysis of the effect of both temporal and spatial sampling frequency on the accuracy of velocity measurements is presented in Codling and Hill (2005).

1.2.2 Number of Detection Channels

As the examples above illustrate, measurements of cells and their behaviors *in vivo* most frequently rely upon the relationships amongst cell types and their environment. Consequently, the number of detection channels should match the number of fluorescent tags. To this extent, a two-cell interaction requires at least two distinct channels in which to collect the fluorescence emissions from two distinct dyes. For example, interactions between T cells and DCs can be achieved using a red fluorophore (e.g., the vital dye CMTMR) to label T cells and the distinct green fluorophore (e.g., CFSE) labeling method for the DCs (Miller et al. 2004).

However, as the compartmentalization of the immune response is studied further, it becomes apparent that even a 'simple' organ like a lymph node comprises distinct zones and behaviors which vary according to those zones. This requires the use of additional fluorophores or combinations of fluorophores to highlight critical regions;

we term this fiduciary labeling as the fluorophore which thus serves to highlight key positions within organs and tissues. So, for example, activating B cells near the T–B border move toward the border as a result of gradients of CCR7 ligands whereas those that are a distance away fail to do so – despite both being within the same B cell follicle (Okada et al. 2005). Additional fluorophores that highlight this border (in this case those that highlight the T cell zone) prove useful in determining the spatially distinct behavior. As another example, T cells in ectopic EL-4 tumors tend to migrate along paths parallel to blood vessels. Markers that highlight the blood vessels are necessary to reveal this – otherwise the T cells show guided migration without any mechanistic insight behind the nature of this confinement.

Thus, the use of fiduciary labeling leads to a frequent need to provide at least a third channel. More complex biology (i.e., those involving more than two cell types plus obligate fiduciary labels) can easily require 4 or more channels and this should be considered for choosing or adapting a microscope. In practice, the number of fluorophores and thus channels does not need to equal the number of distinct species to be labeled due to the possibility for multiplexing. In this way, three cell types can be labeled using combinations of just two dyes (green, red and green–red together create three distinct species in just two channels). As a general rule, the number of populations that can be distinctly labeled can be defined as:

$$C = 2^n - 1$$

where *C* is the number of distinct species that can be separately distinguished based on binary determinations of the presence of a dye and n is the number of channels of distinct detection. In practice, the true number that can be distinguished depends a bit on the application. For example, if labeled species (e.g., cells) never get very close, then different levels of each dye can be introduced into collections of cells leading to much larger variation in species and thus discrimination. As an example, Lichtman and colleagues generated populations of neurons *in vivo* using differing levels of CFP, YFP, and dsRed (three fluorophores) which permitted discrimination of approximately 90 different ‘colors’ based on combinations of just these three (Livet et al. 2007). On the other hand, the ability to discriminate based on quantitative measures of each component (component analysis) is made more difficult by fluorophores with wide-emissions that ‘bleed’ light into each other’s emission channels and thus somewhat resemble ‘dual-colored species’. Component analysis can often still distinguish these, except when cells or structures bearing fluorophores get very close to one another. When species overlap in the same measurement space (i.e., voxel), the quantitative contributions also blur and it is often difficult to tease apart the borders of the two. Under such circumstances, more distinct fluorophores may be required.

1.2.3 Detection Sensitivity

A critical requirement for effective deep-tissue imaging of immune cells is efficient detection of emission light. There are two aspects of detection sensitivity: detector sensitivity and detection path efficiency. In general, there are two main detector options:

photomultiplier tubes (PMTs) and charge-coupled device (CCD) cameras. CCD cameras typically have better quantum efficiency, the ability to convert light into electrical signals suitable to digitize. However, while both detector types can have high gain capabilities, PMTs often excel in multichannel and scanning applications because they combine good sensitivity with a large measurement bandwidth. PMT-based systems are also less affected by scattering in the emission path because fluorescence is assigned to a particular point in the sample based on its instantaneous excitation time rather than by its position at the detector. Additionally, PMT number scales more cheaply than increases in camera number. This is particularly important for systems employing three or four emission channels. While it is possible to combine a CCD camera with an emission filter wheel to get spectral separation this results in considerably higher total collection times since each volume of data needs to be illuminated multiple times. This in turn can affect the overall collection speed and increase the likelihood of photobleaching and phototoxicity at the sample.

The nature of the detection path also determines the collection efficiency of the optical system and is therefore an important parameter. The detection path extends from the back aperture of the objective lens through to the detector itself. From an optical design perspective, short detection paths generally provide the greatest collection efficiency. Furthermore, the correct choice of dichroic mirrors and barrier filters along this path are critical to maximizing total detection efficiency, minimizing the detection of autofluorescent wavelengths and minimizing bleed-over or crosstalk between emission channels.

1.2.4 Number of Lasers

Another way to distinguish between different fluorescent species (and thereby discriminate between more cell types or fiduciary species) is to employ different excitation wavelengths. Switching between different excitation wavelengths is not easily achieved with current Ti-sapphire lasers. However, we and a number of other groups have begun to integrate multiple lasers into a single system. While not a cheap option, this approach benefits from the ability to excite more fluorophores and distinguish between fluorophores with overlapping emission spectra but resolvable excitation spectra. However, simultaneously illuminating a sample with two lasers increases the likelihood of phototoxicity and complicates the discrimination of fluorophores with overlapping excitation spectra. For this reason, dual or multiple laser systems typically require recording from interlaced frames, which increases the amount of time required to scan the sample and thus decreases the overall collection rate.

1.2.5 Depth Penetration

Much of the interesting biology of the immune response occurs below the surface of organs. Unfortunately, most mammalian tissues scatter visible light significantly

and do so in a wavelength-dependent fashion. Measured scattering constants (μs) are typically of the order of 50 cm^{-1} (Collier et al. 2003). The probability of transmission T of the photon without redirection by scattering after a path length L (cm) is given by the equation:

$$T = e^{-\mu s L}.$$

Under these circumstances, at depths of just 50 μm, approximately 25% of the incident beam is typically scattered (and lost) during excitation and a similar percentage is redirected during fluorescence emission. This rises to 40% at 100 μm and 72% at 250 μm making such depths practically inaccessible.

Additionally, tissue is not just scattering but also absorptive of both incident light and emitted fluorescence, an effect that is linearly related to the tissue thickness (depth) subtended during excitation. Absorption is also highly dependent on the wavelength of incident light (or fluorescence) and is somewhat tissue specific. Typically, visible light is more likely to be absorbed. In fact, it has long been recognized that there exists an "optical window" (i.e., 600–700 nm) where major cell and tissue absorbers, such as melanin and hemoglobin, exhibit the least amount of absorbance (König 2000). This optical window has been exploited by many *in vivo* microscopic techniques (Frangioni 2003).

Scanning of the sample (vs full field illumination), coupled with collection at a PMT, permits spatial assignment of all of the measured emitted light intensity. This occurs regardless of the scattered path this light takes en route to the PMT and thus effectively eliminates a large portion of emission scatter. However, the most critical feature in deep tissue is absorption and this is where many confocal approaches often fail. In practice, imaged depths of up to 100 μm have been reported with spinning disk (Egeblad et al. 2008) or even scanning-based confocal microscopy (Stoll et al. 2002). The former, when operated up to these depths, can sometimes be significantly better than multiphoton imaging as a result of the larger quantum efficiencies of current-generation cascade-based CCD cameras (as compared to PMTs). There can also be some overall benefit in resolution at shallow depths due to the combined effects of lower wavelengths used in single-photon and confocal pinhole on the overall point-spread function. However, starting around 50 μm in many tissues, the scatter into adjacent pixels (blurring) combined with the loss of incident excitation light due to single-photon absorption becomes unacceptably high.

1.3 Advantages of Multiphoton Imaging

While many forms of optical imaging can be used to study the immune system, multiphoton imaging has many clear advantages. These advantages include superior tissue penetration, less image degradation by light scattering leading to better resolution, and high image quality deep inside tissues. Furthermore, tissue autofluorescence elicited with infra-red (IR) excitation is significantly reduced over equivalent visible

Table 1 Current multiphoton instrument options

	Source	Scanning mechanism		Detector	Colors	Sensitivity	Imaging rate (fps)	Spatial resolution (max. lines per image)	Pulse conditioning	Ease of implementing	Cost
		X and Y	Z (range)								
Custom	Parker–Sanderson Krummel–Bullen	Resonant + galvo	Pifoc (350 μm)	PMT	2 4	High	Up to 60	400	No Yes	Difficult Moderate	$$$
	Svoboda	Dual galvo	???	PMT	2	High	2	???	No	Difficult	$$$
	Kleinfield	Dual galvo	Focus drive automation	PMT	2	High	3	512	No	Difficult	$$$
Mixed[1]	Yuste[2]	Dual galvo	Focus drive automation	PMT	1 + 1[3]	High	2	512	No	Moderate	$$$$
	Ridsdale[4]	Dual galvo	Focus drive automation	PMT	3	High	2	512	No	Moderate	$$$$
Commercial	Zeiss LSM 710 NLO	Dual galvo	Piezo (??μm)	PMT	2 or 3	High	5	Up to 6,144 per dimension	Nonstandard	Easy	$$$$$
	Olympus FV1000 MPE	Dual galvo	Focus drive automation	PMT	2	High	4	64–4,096 per dimension	Yes	Easy	$$$$$
	Lecia TCS SP5 MP	Tandem systems[5]	Focus drive automation	PMT	4	High	1[5] or 25[7]	8,196[8] or 512[9]	Nonstandard	Easy	$$$$$
	Prairie Ultima	Tandem systems[10]	Focus drive automation	PMT	2 or 3	High	1[11] or 30[12]	512	Nonstandard	Easy	$$$$
	LaVision TriM Scope	Multibeam	Piezo[13]	CCD camera	1[14]	Low	$30[15]	1,000[16]	Yes	Easy	$$$$$

[1]Adaptation of existing commercial system
[2]Modification of Olympus Fluoview microscope
[3]One detector for fluorescence and one for SHG signal
[4]Modification of Nikon C1 confocal scope
[5]Tandem scanning system includes dual galvos scanner and resonant scanner operating in bidirectional scan mode
[6]Using dual galvo scanner
[7]Using fast resonant scanner
[8]Using dual galvo scanner
[9]Using fast resonant scanner
[10]Tandem scanning system includes dual galvos scanner and acoustic optic scanner.
[11]Using dual galvo scanner
[12]Using acousto optic scanner
[13]Signal limited to first 150 μm
[14]More possible with extra camera and/or emission filter wheel
[15,16]Depends on CCD camera

wavelengths, which improves signal specificity and image brightness against background. When compared to confocal systems, multiphoton systems typically exhibit better optical efficiency with no signal loss arising from an emission pinhole. So, while absolute signal magnitude is typically less when compared to confocal applications, the overall signal-to-noise ratio is typically improved. Multiphoton excitation also produces highly resolved z excitation planes that leads to extremely good z-registration and consequently better three dimensional reconstructions. This localized excitation also produces lower levels of photodamage (i.e., toxicity) and thereby allows increased recording episodes. In short, the tissue penetrating power of infrared light makes multiphoton excitation especially suitable for *ex vivo* and in situ imaging.

Multiphoton imaging systems are available in many forms. These options include commercial systems, user adaptations of existing confocal microscopes, and custom systems. Many of these current options and the relative merits of each type are documented in Table 1. Current commercial two-photon imaging systems are commonly extensions of existing confocal microscopes and therefore enjoy the advantages of being commercial grade instruments with the flexibility to perform different kinds of imaging.

In contrast, custom-built systems can be constructed at a considerably reduced cost and offer greater potential for customization. In particular, they offer the ability to quickly add extra features and improved capabilities. There are also several free software packages [e.g., ScanImage (Pologruto et al. 2003) and MPScope (Nguyen et al. 2006)] available that facilitate the construction of these custom-built systems. Existing confocal microscopes can also be retrofitted by users to become two-photon scopes, and there are several reports documenting how this can be done (e.g., Fan et al 1999; Majewska et al. 2000; Nikolenko et al. 2003; Ridsdale et al. 2004).

2 Description of Custom Two-Photon Instrumentation

We have assembled a scanning two-photon system based on a resonant scanner as first used by Tsien and colleagues (Fan et al. 1999). Our design was modeled after second generation resonant scanner designs by Ian Parker and Mike Sanderson (Sanderson and Parker 2003; Callamaras and Parker 1999). Their early designs functioned as confocal systems but more recent incarnations extend the technology (and actually simplify the design) for two-photon excitation (Nguyen et al. 2001). In addition to minor modifications in the overall design of the Parker/Sanderson prototypes, our instruments have been expanded to include four PMTs and also place those PMTs within the infinity space of the objective. Four-channel collection (and higher channel numbers) are now possible using high-speed acquisition cards. Furthermore, as we are essentially biologists first, our system is facilitated by a collection of scan-head parts available from Sutter Instruments. This availability dramatically reduces the need for novices to construct parts.

2.1 A Custom Design Composed of Off-the-Shelf Parts Simplifies System Construction

The important elements in this design are shown schematically in Fig. 1. Generally, this system can be assembled from readily available parts. Each of these parts and their important properties are discussed below. Additional and more detailed information regarding this design is available on our website (http://pathology.ucsf.edu/krummel/2PhotonHome.html). Included on this site is a comprehensive parts list.

2.1.1 Laser

Highly specialized lasers are required for multiphoton excitation. In particular, this type of excitation requires the concentration of photons in space and time. Spatial concentration of photons is normally achieved by focusing a laser beam to a small spot with a high numerical aperture objective lens as in traditional single-photon microscopy. In contrast, the temporal concentration of photons is accomplished by compressing photons from a continuous source into ultra-short (i.e., femtosecond) pulses. Near-infrared pulses of this type are commonly produced by a Ti-sapphire oscillator driven by a continuous-wave pump laser and typically exhibit high peak intensities but low average power.

Early Ti-sapphire lasers were notable for their limited wavelength range and poor user friendliness. In particular, these early systems were intolerant to variations

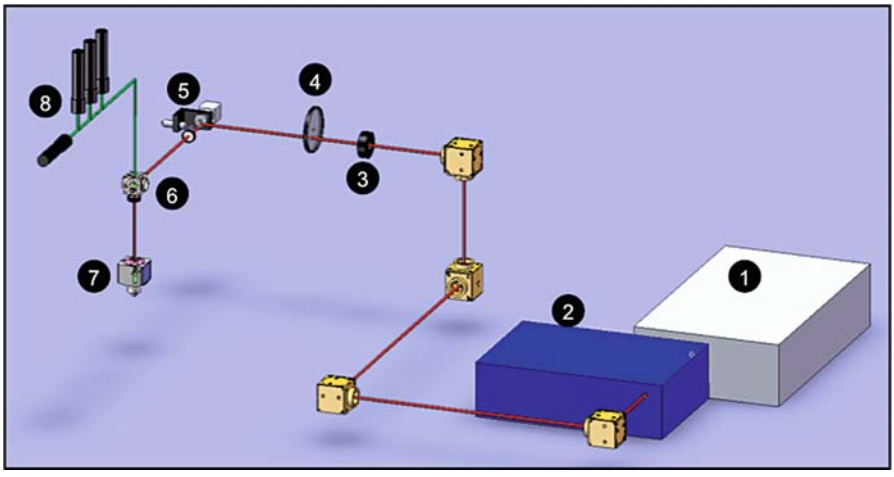

Fig. 1 Instrument design scheme including: (1) Ti–sapphire laser; (2) pulse conditioner; (3) mechanical shutter; (4) neutral density filter wheel; (5) scanning mirrors; (6) primary dichroic mirror; (7) z-focus drive including objective; and (8) PMTs

in room temperature and required constant adjustment. Now, however, there are modern one-box solutions that encompass both the pump laser and the regenerative amplifier which perform more robustly. These systems have simplified laser control and operation to the point where everyday laser operation no longer requires a specialized laser technician.

Likewise, extended range Ti:Sapphire lasers are now available that give access, and sufficient power, to a wider spectral range (700–1,040 nm). This is important for those interested imaging with red fluorescent protein (RFP) and other indicators that require longer excitation wavelengths. This improved spectral bandwidth also enables the use of more fluorophores within the same experiments.

Our multiphoton imaging systems all employ some version of the Newport/Spectraphysics Maitai product, but equivalent lasers from other suppliers are available that perform similarly. This laser has a pulse length of approximately of ~100 fs and is clocked at 80 MHz. Lasers are available that possess shorter pulse lengths and in theory these may improve multiphoton excitation provided that these pulses can be propagated all the way to the sample. These Ti–sapphire systems also come in a range of sizes. Typically, 6-W systems produce sufficient power to support most kinds of imaging. Because of the nature of this laser, and the downstream imaging hardware, it is firmly mounted to a large vibration isolation table.

2.1.2 Pulse Conditioning Unit

Immediately downstream of the laser is a pulse-conditioning unit that prechirps the femtosecond pulses in a way that maximizes the efficiency of multiphoton excitation. The role of this device and its utility is described in a later section. We have employed two different version of this technology: firstly, a freestanding device from APE (Berlin, Germany) called FemtoControl, and secondly, on a separate system, we have installed an add-on called DeepSee, from Newport/Spectraphysics, to an existing Ti–sapphire laser. Both systems are functionally equivalent.

2.1.3 Translation Optics

The beam steering optics used in this design translate the laser beam between devices laid out on a large vibration isolation table. Typically we have chosen to use optical components that are optimized for ultra-fast laser applications (mostly from Newport Corporation). These broadband optics are designed to operate over the spectral range, and at the power levels, of the Ti–sapphire laser while exhibiting maximizing reflectivity and minimizing pulse dispersion.

2.1.4 Scanning Mirrors

The vast majority of laser scanning microscopes use galvanometer mirrors. They have excellent optical properties and allow zooming and image rotation. Their major

drawback is their relatively slow speed (>1 ms per line). Resonant mirrors are an alternative often used for high frame rate imaging. We have chosen to use a dual configuration including a fast (8 kHz) resonant scanner for fast line scans (CRS) and a slower closed-loop galvanometric scanner for vertical scanning (M3S). Bi-directional horizontal scanning enables line scans of approximately ~60 μs in duration which corresponds to video rate imaging with 480 lines per image. We obtained both these scanning mirrors from General Scanning Inc. (GSI; Billerica, MA). Each scanner is under the control of custom electronics also supplied by GSI. These electronics, power supplies and related hardware required to synchronize this system with the video acquisition board are contained within a mirror control box (Sutter Instruments, Novato, CA). These scanners are mounted on an optical breadboard enclosed within a scanning enclosure. This enclosure was also manufactured by Sutter Instruments and is mounted adjacent to Olympus BX51 microscope base.

One problem with these resonant mirrors is that they introduce some image distortion that requires digital correction. This distortion arises because the mirror velocity is not linear but rather has a sinusoidal profile. The pixel manipulation and field selection required to overcome this image distortion is conducted automatically behind the scenes and is transparent to the user. Details of the mathematical procedure underlying this correction have been described extensively elsewhere (Sanderson 2004; Leybaert et al. 2005).

2.1.5 Objectives, Field Size and Stage Movement

The objective lens(es) used with this system determines the level of spatial resolution and the efficiency of signal capture. Any lens considered must also be able to work in media or physiological fluids and possess sufficient working distance for use with tissues and animals. Moreover, it must exhibit high transmittance for both the pulsed IR excitation light and a wide range of emitted fluorescence. We predominantly use an XLUMP FL20XW from Olympus. This objective combines intermediate magnification (20×) with relatively high NA (0.95) and is particularly well suited for imaging in scattering tissue.

This system also possesses electronic control of the field size. The user is able to choose between two pixel sizes (i.e., 0.4 or 0.7 μm pixel^{-1}). Correspondingly, the field size scanned is either 192 × 160 μm or 336 × 280 μm.

While most of the experimental work conducted on this system is focused on a microscopic level of detail, there are instances where users want to combine both microscopic and macroscopic levels of resolution. This is achieved by stage scanning with a motorized stage (Prior 101A, Boston, MA). This process is automated and controlled in software (described below).

2.1.6 PMT Selection

Photomultiplier tubes are hand-made devices with a surprising amount of batch-to-batch variability in their signal- and noise-amplification characteristics. While each supplier typically provides average values for sensitivity and noise performance,

these can be misleading. In particular, root–mean–square (rms) measurements of noise performance are essentially time-averages that disguise significant peak-to-peak signal fluctuations. In high bandwidth applications, such as video rate scanning, short but significant bursts of noise, which are undetectable in rms measurements, become significant problems. For example, in a system collecting pixels at MHz frequency, we have observed PMTs with transient bursts of noise lasting just a microsecond or two that cause isolated pixels to become completely saturated. Depending on the frequency of these bursts, such PMTs may prove unsuitable for imaging. Some suppliers allow batches of 10–20 PMTs to be individually tested as part of a purchase. In general, there continues to be advances in the development of lower-noise, high gain PMTs. For instance, some latest generation GaAs-based detectors have shown exceptional sensitivity and signal-to-noise performance. However, such PMTs can also become easily saturated and transiently insensitive. This places an additional burden on the user to carefully manage their light levels to avoid such damage.

2.1.7 Emission Split Allows Four-Color Imaging

The four emission channels included in this design provide coverage of most of the visual spectrum normally used for fluorescence imaging. A scheme showing the specifics of these individual channels is documented in Fig. 2. The spectral placement of these channels allows one to collect signal from four independent fluorophores. Moreover, the relative placement of these filters was chosen to (1) match the spectra from currently available fluorescent proteins, (2) provide the best spectral separation between fluorophores, and (3) to maximize the signal capture in each channel. With our current hardware, there is some flexibility to switch emission filters and thereby fine-tune these channels even further, but changing dichroic mirrors is more difficult. In cases where the spectra of two fluorophores overlap in adjacent channels, it is possible, via image math, to separate out the underlying contribution of each indicator. Likewise, linear unmixing can be used to remove the contribution of autofluorescence or overlapping signals. Examples of these procedures are shown in below Fig. 6.

2.1.8 Software

Our system employs several different software applications from multiple vendors. These applications are run on two separate computers and in turn connect to several devices or control boxes. A scheme documenting the relationships between these computers, applications and devices is shown in Fig. 3. Coordination of these disparate elements during image acquisition is achieved by a single master application (Confocal; IO Industries, London, Ontario, Canada). The Confocal application controls the scheduling and relative timing of all the hardware devices used in a typical experiment. It also interacts with a commercial video recording software suite (i.e., VideoSavant) that is used to reconstruct and record images.

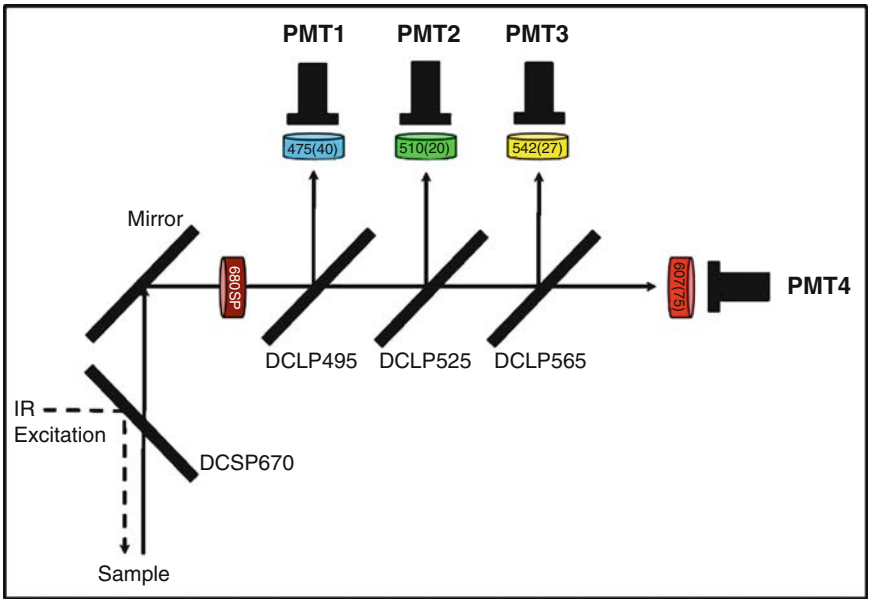

Fig. 2 Emission split. This optical configuration is optimized to capture the maximum fluorescence signal from commonly used fluorescence proteins (especially CFP, GFP, YFP and dsRed or similar). This setup includes a strong excitation blocking filter that excludes any backscattered excitation light without impacting the emitted fluorescence. *DCSP* Dichroic short-pass mirror, *DCLP* dichroic long-pass mirror. Barrier filters described by their center wavelength (and full width at half maximum)

The graphical user interfaces of these programs are shown in Fig. 4. The confocal application is composed of a Main tab and three derivative tabs. Data can be acquired as a single time point, a z-series, a z-series over time, or any of the above using multiple stage positions. Files are exported in multiimage TIFF format that is accessible to Image J, Metamorph, Imaris, and the simpler Windows image viewers.

2.2 Optimizing Two-Photon Instrumentation

It is relatively common nowadays to be able to buy, or retrofit, an existing confocal microscope with a laser suitable for multiphoton excitation. However, such instruments provide relatively poor imaging capabilities and many are unable to achieve the necessary frames rates described earlier. Furthermore, the relative efficiency of IR delivery and fluorescence capture in these systems is often suboptimal. Based on these factors and others we have learned from experience, the following section describes several critical considerations in achieving high quality multiphoton images and physiologically relevant results.

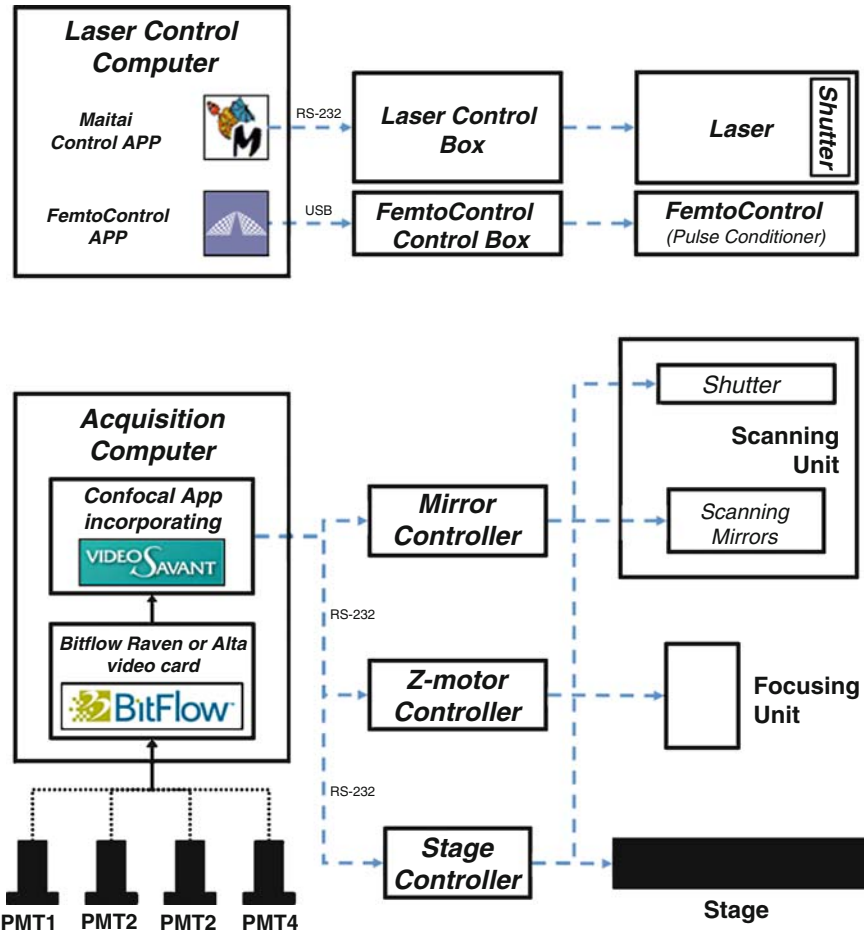

Fig. 3 Software control scheme showing the relationship between the acquisition and laser control computers, device control boxes and each physical device in the larger system. *Dotted blue lines* represent outbound control signals. *Black lines* represent acquired or processed signals

2.2.1 A Simplified Light Path Minimizes the Effect of Dispersion

The strength of multiphoton excitation is inversely proportional to pulse duration. Although very short pulses (<100 fs) give the strongest signal, they are no longer purely monochromatic and, as they propagate through different optical elements (i.e., optical fibers and objective lens), some dispersion, or pulse broadening, occurs. This chromatic dispersion arises because separate spectral components are retarded differentially depending on their wavelength. Pulse dispersion reduces the overall efficiency of multiphoton excitation in general but is most

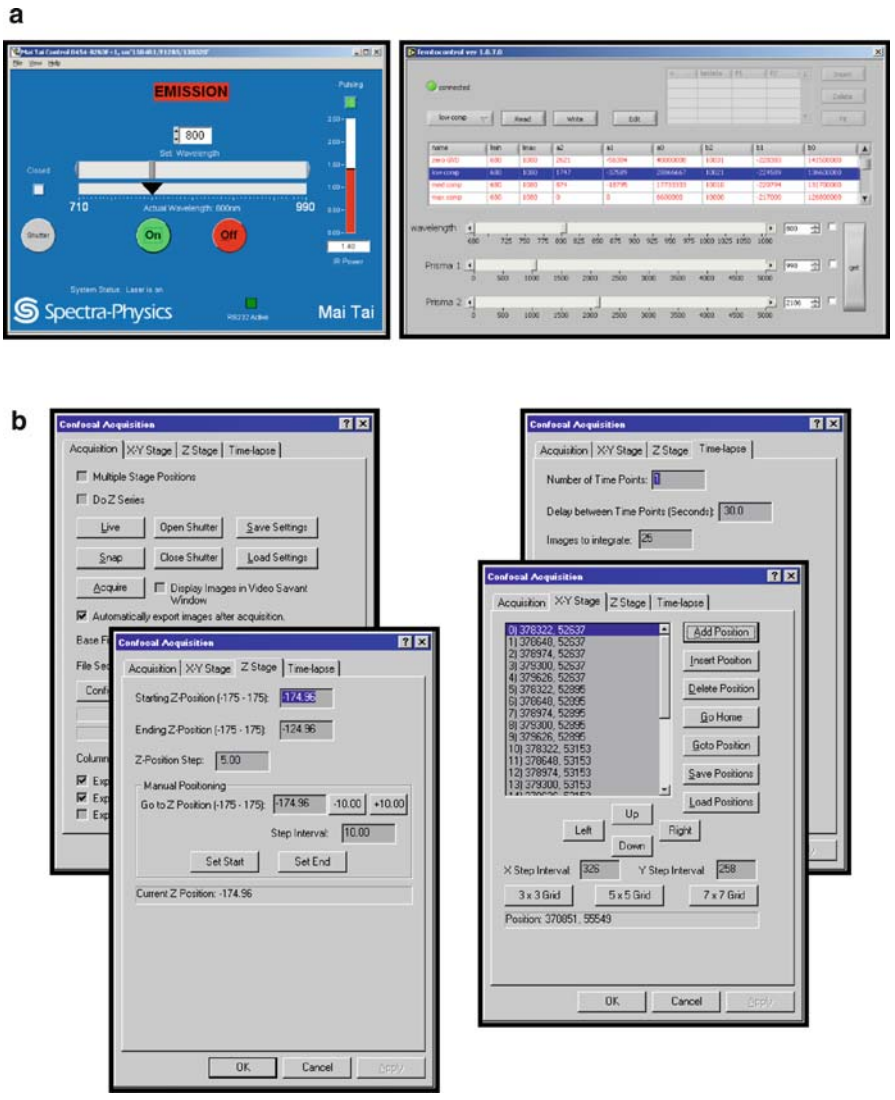

Fig. 4 Software user interface. (**a**) Applications running on the laser control computer. (**b**) Different control tabs of the Confocal application running on the acquisition computer

problematic in applications that use complicated optical configurations such as intravital microscopy (IVM). In theory, pulses of greater starting intensity could be used to overcome dispersion, but these can cause photodamage. Similarly, pulse power can be amplified at the expense of repetition rate (Theer et al. 2003) but again, only under conditions in which photodamage or background fluorescence are not limiting.

It should be noted that simpler optical systems limit dispersion because they have fewer optical elements (lenses, mirrors, etc.) which are the primary site where dispersion arises. Since a dedicated two-photon instrument can be easily assembled with only a few optical elements (the required light path consists of approximately 3 cm of glass), dispersion can be kept low and excitation maximal. Thus, our strategy to overcome the effects of pulse dispersion is to minimize amount of glass in the system, but obviously some glass is always required. In contrast, many recent commercial systems have suffered from the use of highly dispersive elements, notably large numbers of relay lenses as well as dispersive elements such as acousto–optic deflectors (AODs). The resultant loss in peak power made many of these extremely inefficient at producing the high peak powers that is necessary for producing the two-photon effect.

2.2.2 Pulse Conditioning can be Used to Overcome the Effect of Dispersion

New methods of pulse shaping are now available that completely counteract pulse dispersion and thereby improve the efficiency of multiphoton imaging. Pulse-shaping methods (also called prechirping) impart a 'negative dispersion' (also known as negative group velocity dispersion or GVD) to longer wavelength components in each pulse and thereby allow pulses to travel further through a scattering tissue before they become too weak to be effective (Fig. 5a). This manipulation improves the effective depth penetration by up to three times (McConnell 2006) relative to unconditioned pulses without causing any additional photodamage. In general, pulse compression produces better images by optimizing multiphoton excitation. Some tissues may also add additional dispersion effects such as bone when imaging through the skull or various connective tissues capsules around other organs. Unexpectedly, there are even reports that relatively simple biological fluids can also add small amounts of pulse dispersion (Coello et al. 2007). Additional dispersion compensation can be used to overcome these tissue and fluids effects. Commercial devices are now available that precondition pulses for dispersion compensation and many of these are now being built into one-box laser solutions (e.g., Maitai DeepSee).

2.2.3 Resonant Scanning is Required to Achieve High Frame Rates

A majority of commercial multiphoton instruments typically scan the sample on-demand. For most commercial systems, the slow rate of scanning mirror movement, and other factors, conspire to limit the image acquisition to approximately 1–4 s per image. In contrast, a resonant scanner is always oscillating at a higher rate and much higher frame rates are easily achieved. If this higher frame is not required then multiple frames can be averaged to increase the signal-to-noise ratio. The version that we utilize typically produces an image of 400 × 480 pixels 30 times per second. When these scanners are coupled with fast piezoelectric z-drives (with settling times of approximately 10 ms) the result is effectively 3–6 z-sections per second,

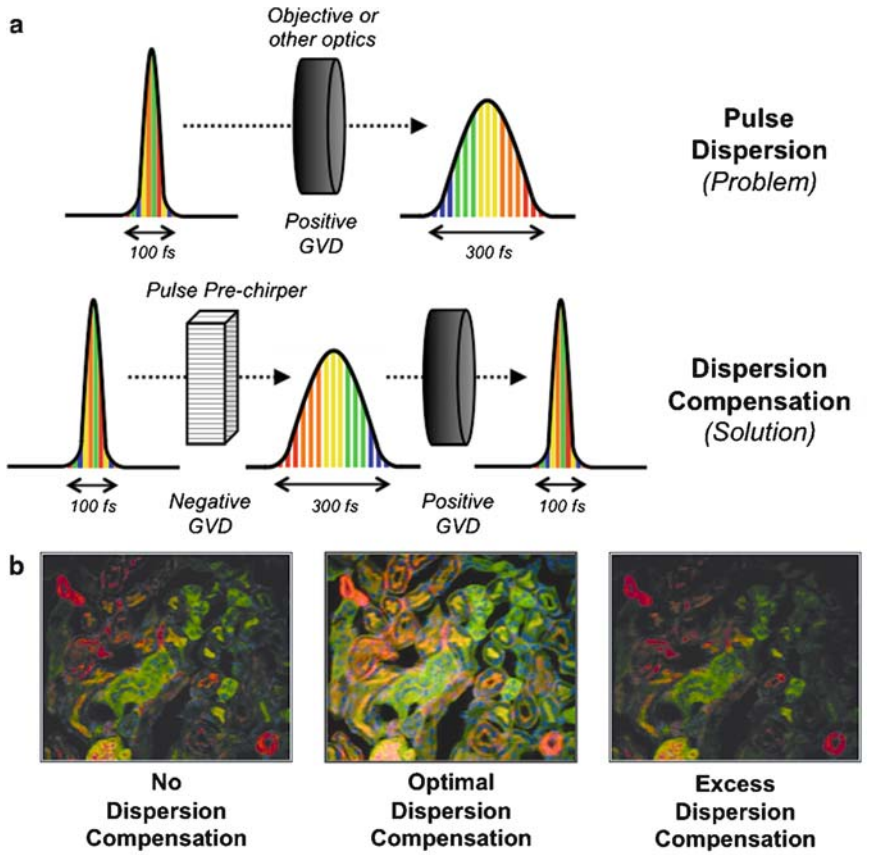

Fig. 5 Pulse compression for improved image brightness. (**a**) Illustrates the problem of pulse dispersion whereby system optics smear and attenuate laser pulses. Pulse chirping preconditions these pulses so that when they reach the sample they are in an optimal form for two-photon excitation. (**b**) Representatives with and without dispersion compensation

which is a dramatic improvement over conventional scanning modes. One downside of this technology is that the scanning pattern is relatively fixed. There is little scope for zooming or scanning smaller regions of interest. This rules out FRAP-type bleaching or faster scanning of smaller regions. However, in practice, this limitation is not significant for many current *in vivo* applications where FRAP has not yet seen great utility and where large fields are desirable.

2.2.4 Frame Averaging can Improve Image Quality

Video-rate image capture sometimes suffers from diminished image quality, especially when the underlying signal is weak. This occurs because pixel dwell times are

typically quite short in comparison to nonresonant scanning technologies. Frame averaging can be used to overcome this problem. The extent of signal improvement is governed by sampling theory and therefore significant image improvements can be achieved by averaging 5–30 frames. Further averaging typically produces only small improvements in image quality and this occurs at the expense of increase exposure times. In practice, most applications require some amount of frame-averaging (typically 5–20 frames averaged) resulting in effective frame rates of 3–12 frames per second.

2.2.5 Maintaining Tissue Viability and Animal Health

We (Friedman et al. 2005) and others (Miller et al. 2002) have shown that various aspects of immune physiology are exquisitely sensitive to variations in temperature and oxygen concentration. For this reason, it is important to carefully monitor and control the temperature and oxygenation state of any tissue being examined with two-photon microscopy. Numerous commercial systems are readily available for this purpose. Likewise, if mice or other whole animals are being studied, it is critical to control their temperature, respiration, and state of anesthesia.

3 Representative Data

Our four-channel TPLSM system has recently allowed us (Gardner et al. 2008) to image three unique cell populations and the lymph node capsule, as well as to isolate our fluorescent signals from the autofluorescence present in the tissue (See Fig. 6). In this example, the collagen capsule is visualized by using collagen's second harmonic generation, leaving three channels available to detect our labeled cell populations.

In the examples shown in Fig. 6, transgenic Adig mice express IGRP–GFP under the Aire promoter in mTECs (medullary thymic epithelial cells) and in a population of cells in secondary lymphoid organs termed eTACs (extra-thymic Aire-expressing cells). GFP expression levels in eTACs are low, especially when compared to the high levels of green autofluorescence in the region of the lymph node where these cells are present. While the GFP fluorescence is primarily present in the green channel, the tissue autofluorescence is more broadly detectable. This allowed us to use image math to eliminate the autofluorescent signal from the green channel that obscured the GFP signal (Fig. 6a).

The goal of these studies was to analyze the interactions between T cells and eTACs (Gardner et al.2008). Since T cell behavior varies depending on microenvironment, often the best control is to simultaneously image control cell populations in the same microenvironment as experimental cell populations. To image control and experimental T cell populations together with the GFP labeled eTACs and the second harmonic, we labeled one population of T cells with CMTMR and the second with both CMTMR and CFSE. By separating out the dually labeled cells based

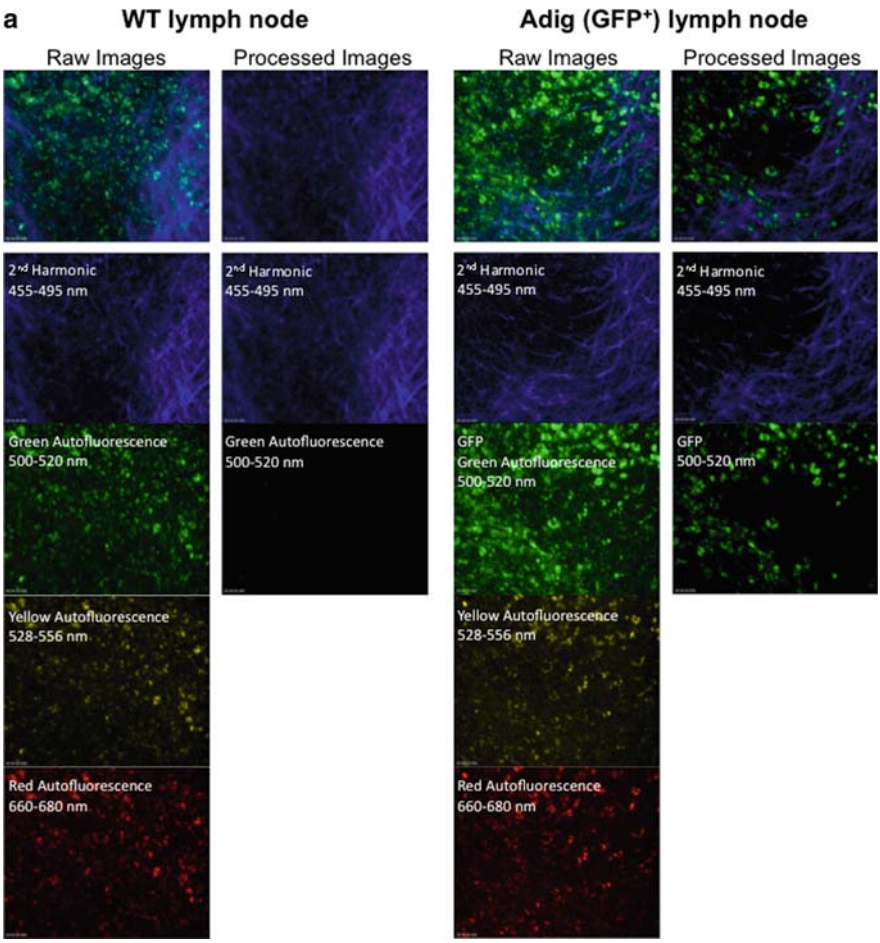

Fig. 6 Representative data. **(a)** Using autofluorescent signals in unused channels to eliminate autofluorescence in the channel of interest. Images show maximum intensity *Z* projections of florescence levels in the blue and green channels overlayed (*top*), and in individual channels (*bottom*) before and after image processing. The green (500–520 nm) channel contained a large amount of autofluorescent signal that obscured the dim GFP signal. The autofluorescence was also present in the yellow (528–556 nm) and red (660–680 nm) channels, while the GFP signal was primarily present in the green channel. Using a sample without GFP fluorescence (*left*) we established an equation to subtract out the autofluorescent signal where "*a*" was determined based on the overlap between autofluorescence in the green and yellow channels and "*b*" was determined based on the overlap between the green and red channels.

$$\text{GFP Fluorescence} = \text{Green Fluorescence} - a \times \text{Yellow Fluorescence} - b \times \text{Red Fluorescence}$$

When applied to a sample without GFP fluorescence this equation eliminated the green autofluorescence (*left*), and when applied to a sample containing GFP labeled cells (*right*), the equation eliminated autofluorescence without eliminating GFP fluorescence, making the GFP signal clearly identifiable. Following image arithmetic to eliminate autofluorescence, the images were processed with a Gaussian filter to reduce noise. Image processing was done using Imaris and Matlab.

on the colocalization of emission in the red and green channels, and subsequently applying image arithmetic, we were able to isolate the signals from each of the cell populations and the second harmonic into four unique channels (Fig. 6b).

4 Future Perspectives

4.1 Pulse Manipulations

In addition to the femtosecond pulse manipulations described earlier, there have been a number recent advances that further enhance signal intensity and/or reduce phototoxicity. Some these advances are described below. Adoption of these are likely to further expand the utility of TPLSM in the future.

Fig. 6 (continued) (b) Using image arithmetic to separate populations with different fluorescence profiles. As described in Fig. 6a, the dim GFP signal is obscured by strong autofluorescence in the green channel. Additionally, two populations of T cells were added to the sample. One population was labeled with the dye CMTMR which is detected in the red channel, and the other population was labeled with both CMTMR which is detected in the red channel and CFSE which is detected in the green and yellow channels. Our goal was to establish clearly separated channels for each of the three cell populations and to eliminate autofluorescence. To do this, we first established a new channel that contained the regions of bright colocalized green and red fluorescence, where "*c*" and "*d*" were determined based on the fluorescent levels of the CMTMR/CFSE labeled cells in the red and green channels respectively.

Colocalized CMTMR/CFSE Fluorescence = Pixels with Red > *c* and Green > *d*

This channel specifically contained the T cell population that was labeled with both CMTMR and CFSE dyes. The equation previously established to eliminate autofluorescence in the green channel was then applied.

GFP Fluorescence = Green Fluorescence – $a \times$ Yellow Fluorescence – $b \times$ Red Fluorescence

In this case, the equation served to both eliminate green autofluorescence and to eliminate fluorescence in the green channel from the CMTMR/CFSE labeled cell population, leaving only the GFP signal in the green channel. We then applied an equation to eliminate autofluorescence in the red channel, as well as to eliminate fluorescence in the red channel from the CMTMR/CFSE labeled cell population where "*e*" was determined based on the overlap between autofluorescence and CMTMR/CFSE fluorescence in the red and yellow channels and "*f*" was determined based on the overlap between the red and green channels.

CMTMR Fluorescence = Red Fluorescence – $e \times$ Yellow Fluorescence – $f \times$ Green Fluorescence

When applied to the sample this equation eliminated autofluorescence and fluorescence from the CMTMR/CFSE labeled cell population without eliminating fluorescence from the cell population labeled with only CMTMR. Following image arithmetic to separate the cell populations and eliminate autofluorescence, the images were processed with a Gaussian filter to reduce noise. Image processing was done using Imaris and Matlab

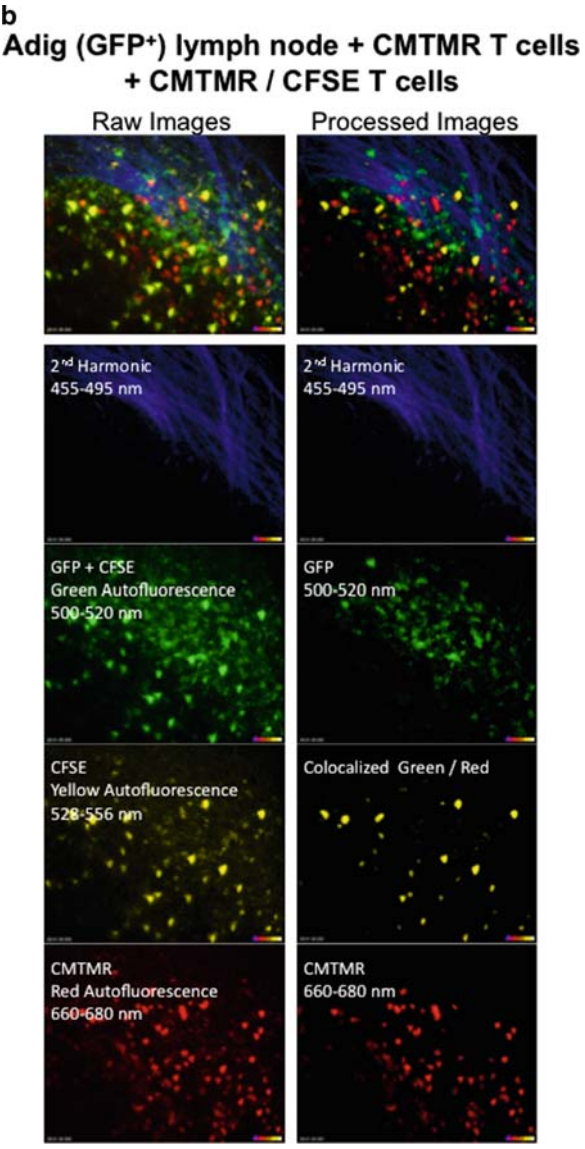

Fig. 6 (continued)

4.1.1 Increasing the Efficiency of Multiphoton Excitation by Manipulating the Spacing Between Pulses

Donnert and colleagues (Donnert et al. 2007) have recently reported that a substantial improvement in multiphoton efficiency (that is, stronger fluorescence and less photobleaching) could be achieved by increasing the time between successive pulses enough to allow complete dark-state relaxation. Normally, the time between successive pulses in two-photon microscopy is 10–25 ns. By lengthening this time to >1 μs these authors were able to show a substantial augmentation (that is, 20–25×) in fluorescence intensity and significantly less photobleaching. Although this lengthened interpulse interval will probably translate into fewer pulses per pixel dwell time and/or slower frame rates, the magnitude of this signal augmentation is highly significant and will certainly improve image quality in many applications.

4.1.2 Passive Pulse Splitting can also be Used to Enhance Signal Intensity and Reduce Phototoxicity

Magee and Betzig have recently documented a passive pulse splitting strategy whereby each femtosecond pulse is split into many mini-pulses (Ji et al. 2008). These streams of mini-pulses prove to be substantially more efficient for multiphoton excitation (up to 100-fold). Concurrently, these authors described a corresponding 6- to 20-fold decrease in photodamage.

4.1.3 Higher Order, or Pulse Phase, Manipulations can also Help Improve the Effectiveness and Repeatability of Ultra-Short Pulses

These coherence, or phase adjustments, minimize constructive/destructive interference normally occurring within each pulse and thereby promote more homogeneous excitation. Apparently, these phase corrections can increase signal intensity and improve contrast compared with uncompensated pulses. Conveniently, these coherence manipulations are maintained following passage through scattering tissues (Dela Cruz et al. 2004) and there is evidence to suggest that photodamage is also lessened. Interestingly, this method can also be used for selective excitation (Schelhas et al. 2006) of closely spaced fluorophores or ratiometric imaging of different excitation bands.

4.2 Alternative Scanning Methods

Adaptive illumination is a relatively new technique that varies laser intensity with depth and thereby counteracts the effect of decreasing excitation strength with

increasing depth. It has been used in other types of imaging, especially confocal microscopy. Under this scheme, multiphoton excitation is enhanced at the points beyond the normal depth penetration (Chu et al. 2007). Because multiphoton excitation only occurs in a small focal volume the extra energy does not cause any deleterious effects. The profile of increased laser intensity used by this technique can typically be determined empirically, although most often a simple linear ramp is sufficient to produce consistent signal quality improvements at greater depths than usually possible.

Another particularly exciting development in ultra-short pulse-shaping technologies is that some variations may enable axial focusing without having to move the terminal focusing element (that is, without moving an objective lens) (Zhu et al. 2005). In fact, it has been shown that under specific optical conditions insertion of a variable GVD can be used to adjust z-focus. Such a remote axial focusing capability would be a major improvement to current methods in three-dimensional IVM. It may be possible to use this method in combination with lower numerical aperture lenses, which possess correspondingly longer working distances, to reach previously inaccessible tissue depths. Other configurations (Helmchen and Denk 2005) that reduce the effective numerical aperture of an objective (that is, by incompletely illuminating its back focal plane) are also candidates to combine with this temporal focusing effect.

Finally, recent reports (Duemani Reddy et al. 2008; Reddy and Saggau 2005; Saggau 2006) have highlighted the possibility that advanced three-dimensional acousto–optic scanning methods may be applied in multiphoton microscopy. The utility of these methods is that they supposedly allow very fast beam positioning in three-dimensional space without any mechanical movement of scanning mirrors or objectives lenses.

References

Bajenoff M, Egen JG, Koo LY, Laugier JP, Brau F, Glaichenhaus N, Germain RN (2006) Stromal cell networks regulate lymphocyte entry, migration, and territoriality in lymph nodes. Immunity 25:989–1001

Beuneu H, Garcia Z, Bousso P (2006) Cutting edge: cognate CD4 help promotes recruitment of antigen-specific CD8 T cells around dendritic cells. J Immunol 177:1406–1410

Bousso P, Robey E (2003) Dynamics of CD8(+) T cell priming by dendritic cells in intact lymph nodes. Nat Immunol 4:579–585

Bunnell SC, Kapoor V, Trible RP, Zhang W, Samelson LE (2001) Dynamic actin polymerization drives T cell receptor-induced spreading: a role for the signal transduction adaptor LAT. Immunity 14:315–329

Cahalan M, Parker I (2008) Choreography of cell motility and interaction dynamics imaged by two-photon microscopy in lymphoid organs. Annu Rev Immunol 26:585–626

Cahalan MD, Parker I, Wei SH, Miller MJ (2002) Two-photon tissue imaging: seeing the immune system in a fresh light. Nat Rev Immunol 2:872–880

Callamaras N, Parker I (1999) Construction of a confocal microscope for real-time x-y and x-z imaging. Cell Calc 26:271–279

Castellino F, Huang AY, Altan-Bonnet G, Stoll S, Scheinecker C, Germain RN (2006) Chemokines enhance immunity by guiding naive CD8 + T cells to sites of CD4 + T cell-dendritic cell interaction. Nature 440:890–895

Chu K, Lim D, Mertz J (2007) Enhanced weak-signal sensitivity in two-photon microscopy by adaptive illumination. Opt Lett 32:2846–2848

Codling E, Hill N (2005) Sampling rate effects on measurements of correlated and biased random walks. J Theor Biol 233:573–588

Codling E, Plank M, Benhamou S (2008) Random walk models in biology. J R Soc Interf 5:813–834

Coello Y, Xu B, Miller T, Lozovoy V, Dantus M (2007) Group-velocity dispersion measurements of water, seawater, and ocular components using multiphoton intrapulse interference phase scan. Appl Opt 46:8394–8401

Collier T, Arifler D, Malpica A, Follen M, Richards-Kortum R (2003) Determination of Epithelial Tissue Scattering Coefficient Using Confocal Microscopy. IEEE J Sel Top Quant Electr 9:307–313

Dela Cruz J, Pastirk I, Comstock M, Lozovoy V, Dantus M (2004) Use of coherent control methods through scattering biological tissue to achieve functional imaging. Proc Natl Acad Sci USA 101:16996–17001

Delon J, Bercovici N, Liblau R, Trautmann A (1998) Imaging antigen recognition by naive CD4 + T cells: compulsory cytoskeletal alterations for the triggering of an intracellular calcium response. Eur J Immunol 28:716–729

Delon J, Bercovici N, Raposo G, Liblau R, Trautmann A (1998) Antigen-dependent and -independent Ca2 + responses triggered in T cells by dendritic cells compared with B cells. J Exp Med 188:1473–1484

Delon J, Gregoire C, Malissen B, Darche S, Lemaltre F, Kourilsky P, Abastado JP, Trautmann A (1998) CD8 expression allows T cell signaling by monomeric peptide-MHC complexes. Immunity 9:467–473

Donnert G, Eggeling C, Hell S (2007) Major signal increase in fluorescence microscopy through dark-state relaxation. Nat Methods 4:81–86

Duemani Reddy G, Kelleher K, Fink R, Saggau P (2008) Three-dimensional random access multiphoton microscopy for functional imaging of neuronal activity. Nat Neurosci 11:713–720

Dustin ML, Bromley SK, Kan Z, Peterson DA, Unanue ER (1997) Antigen receptor engagement delivers a stop signal to migrating T lymphocytes. Proc Natl Acad Sci USA 94:3909–3913

Egeblad M, Ewald A, Askautrud H, Truitt M, Welm B, Bainbridge E, Peeters G, Krummel M, Werb Z (2008) Visualizing stromal cell dynamics in different tumor microenvironments by spinning disk confocal microscopy. Dis Models Mech 1:155–167

Fan G, Fujisaki H, Miyawaki A, Tsay R, Tsien R, Ellisman M (1999) Video-rate scanning two-photon excitation fluorescence microscopy and ratio imaging with cameleons. Biophys J 76:2412–2420

Frangioni J (2003) In vivo near-infrared fluorescence imaging. Curr Opin Chem Biol 7:626–634

Friedman RS, Jacobelli J, Krummel MF (2005) Mechanisms of T cell motility and arrest: deciphering the relationship between intra- and extracellular determinants. Semin Immunol 17:387–399

Gardner J, Devoss J, Friedman R, Wong D, Tan Y, Zhou X, Johannes K, Su M, Chang H, Krummel M, et al (2008) Deletional tolerance mediated by extrathymic Aire-expressing cells. Science 321:843–847

Helmchen F, Denk W (2005) Deep tissue two-photon microscopy. Nat Methods 2:932–940

Hugues S, Fetler L, Bonifaz L, Helft J, Amblard F, Amigorena S (2004) Distinct T cell dynamics in lymph nodes during the induction of tolerance and immunity. Nat Immunol 5:1235–1242

Hugues S, Scholer A, Boissonnas A, Nussbaum A, Combadiere C, Amigorena S, Fetler L (2007) Dynamic imaging of chemokine-dependent CD8 + T cell help for CD8 + T cell responses. Nat Immunol 8:921–930

Ji N, Magee J, Betzig E (2008) High-speed, low-photodamage nonlinear imaging using passive pulse splitters. Nat Methods 5:197–202

König K (2000) Multiphoton microscopy in life sciences. J Microsc 200:83–104

Krummel MF, Sjaastad MD, Wülfing C, Davis MM (2000) Differential Assembly of CD3z and CD4 During T cell Activation. Science 289:1349–1352

Leybaert L, de Meyer A, Mabilde C, Sanderson M (2005) A simple and practical method to acquire geometrically correct images with resonant scanning-based line scanning in a custom-built video-rate laser scanning microscope. J Microsc 219:133–140
Lindquist RL, Shakhar G, Dudziak D, Wardemann H, Eisenreich T, Dustin ML, Nussenzweig MC (2004) Visualizing dendritic cell networks in vivo. Nat Immunol 5:1243–1250
Livet J, Weissman T, Kang H, Draft R, Lu J, Bennis R, Sanes J, Lichtman J (2007) Transgenic strategies for combinatorial expression of fluorescent proteins in the nervous system. Nature 450:56–62
Majewska A, Yiu G, Yuste R (2000) A custom-made two-photon microscope and deconvolution system. Pflugers Arch 441:398–408
McConnell G (2006) Improving the penetration depth in multiphoton excitation laser scanning microscopy. J Biomed Opt 11:054020
Mempel TR, Henrickson SE, von Andrian UH (2004) T-cell priming by dendritic cells in lymph nodes occurs in three distinct phases. Nature 427:154–159
Miller MJ, Safrina O, Parker I, Cahalan MD (2004) Imaging the single cell dynamics of CD4 + T cell activation by dendritic cells in lymph nodes. J Exp Med 200:847–856
Miller MJ, Wei SH, Parker I, Cahalan MD (2002) Two-photon imaging of lymphocyte motility and antigen response in intact lymph node. Science 296:1869–1873
Negulescu PA, Krasieva TB, Khan A, Kerschbaum HH, Cahalan MD (1996) Polarity of T cell shape, motility, and sensitivity to antigen. Immunity 4:421–430
Nguyen Q, Tsai P, Kleinfeld D (2006) MPScope: a versatile software suite for multiphoton microscopy. J Neurosci Methods 156:351–359
Nguyen QT, Callamaras N, Hsieh C, Parker I (2001) Construction of a two-photon microscope for video-rate Ca(2+) imaging. Cell Calc 30:383–393
Nikolenko V, Nemet B, Yuste R (2003) A two-photon and second-harmonic microscope. Methods 30:3–15
Okada T, Miller MJ, Parker I, Krummel MF, Neighbors M, Hartley SB, O'Garra A, Cahalan MD, Cyster JG (2005) Antigen-engaged B cells undergo chemotaxis toward the T zone and form motile conjugates with helper T cells. PLoS Biol 3:e150
Othmer H, Dunbar S, Alt W (1988) Models of dispersal in biological systems. J Math Biol 26:263–298
Phan TG, Grigorova I, Okada T, Cyster JG (2007) Subcapsular encounter and complement-dependent transport of immune complexes by lymph node B cells. Nat Immunol 8:992–1000
Poenie M, Tsien RY, Schmitt-Verhulst AM (1987) Sequential activation and lethal hit measured by [Ca2+]i in individual cytolytic T cells and targets. EMBO J 6:2223–2232
Pologruto T, Sabatini B, Svoboda K (2003) ScanImage: flexible software for operating laser scanning microscopes. Biomed Eng Online 2:13
Qi H, Egen J, Huang A, Germain R (2006) Extrafollicular activation of lymph node B cells by antigen-bearing dendritic cells. Science 312:1672–1676
Reddy G, Saggau P (2005) Fast three-dimensional laser scanning scheme using acousto-optic deflectors. J Biomed Opt 10:064038
Ridsdale A, Micu I, Stys P (2004) Conversion of the Nikon C1 confocal laser-scanning head for multiphoton excitation on an upright microscope. Appl Opt 43:1669–1675
Sabatos CA, Doh J, Chakravarti S, Friedman RS, Prandurangi PG, Tooley AJ, Krummel MF (2008) A synaptic basis for paracrine interleukin-2 signalling during homotypic T cell interaction. Immunity 29:238–248.
Saggau P (2006) New methods and uses for fast optical scanning. Curr Opin Neurobiol 16:543–550
Sanderson MJ, Parker I (2003) Video-rate confocal microscopy. Methods Enzymol 360:447–481
Sanderson MJ (2004) Acquisition and correction of multiple real-time images for laser-scanning microscopy. Microsc Anal 18:17–23
Schaefer BC, Marrack P, Fanger GR, Kappler JW, Johnson GL, Monks CRF (1999) Live cell fluorescence imaging of T cell MEKK2: Redistribution and activation in response to antigen stimulation of the T cell receptor. Immunity 11:411–421
Schelhas L, Shane J, Dantus M (2006) Advantages of ultrashort phase-shaped pulses for selective two-photon activation and biomedical imaging. Nanomedicine 2:177–181

Shakhar G, Lindquist RL, Skokos D, Dudziak D, Huang JH, Nussenzweig MC, Dustin ML (2005) Stable T cell-dendritic cell interactions precede the development of both tolerance and immunity in vivo. Nat Immunol 6:707–714

Stoll S, Delon J, Brotz TM, Germain RN (2002) Dynamic imaging of T cell-dendritic cell interactions in lymph nodes. Science 296:1873–1876

Tang Q, Adams JY, Tooley AJ, Bi M, Fife BT, Serra P, Santamaria P, Locksley RM, Krummel MF, Bluestone JA (2006) Visualizing regulatory T cell control of autoimmune responses in nonobese diabetic mice. Nat Immunol 7:83–92

Theer P, Hasan M, Denk W (2003) Two-photon imaging to a depth of 1000 microm in living brains by use of a Ti:Al2O3 regenerative amplifier. Opt Lett 28:1022–1024

Varma R, Campi G, Yokosuka T, Saito T, Dustin ML (2006) T cell receptor-proximal signals are sustained in peripheral microclusters and terminated in the central supramolecular activation cluster. Immunity 25:117–127

Williams R, Zipfel W, Webb W (2001) Multiphoton microscopy in biological research. Curr Opin Chem Biol 5:603–608

Wülfing C, Rabinowitz JD, Beeson C, Sjaastad MD, McConnell HM, Davis MM (1997) Kinetics and extent of T cell activation as measured with the calcium signal. J Exp Med 185:1815–1825

Yokosuka T, Sakata-Sogawa K, Kobayashi W, Hiroshima M, Hashimoto-Tane A, Tokunaga M, Dustin ML, Saito T (2005) Newly generated T cell receptor microclusters initiate and sustain T cell activation by recruitment of Zap70 and SLP-76. Nat Immunol 6:117–127

Zhu G, van Howe J, Durst M, Zipfel W, Xu C (2005) Simultaneous spatial and temporal focusing of femtosecond pulses. Opt Exp 13:2153–2159